

Raman scattering in a d-wave superconductor - a one gap scenario

A. V. Chubukov¹ and M. R. Norman²

¹*Department of Physics, University of Wisconsin, Madison, WI 53706*

²*Materials Science Division, Argonne National Laboratory, Argonne, Illinois 60439*

(Dated: November 10, 2018)

Recent Raman scattering data in B_{1g} and B_{2g} geometries in the superconducting state of underdoped cuprates were interpreted as evidence for two distinct energy gaps. We argue that these data can be equally well explained within a one gap scenario if final state interactions are taken into account. In particular, we show that they can account for the differing doping dependences of the Raman peaks in these two geometries.

PACS numbers: 74.20.-z, 74.25.Gz, 74.72.-h

I. INTRODUCTION

A key issue in the physics of cuprates is the relation between the pseudogap and the superconducting gap¹. One class of theories implies that the pseudogap and the superconducting gap are of different origin. The pseudogap appears at T^* in the antinodal region as a result of some competing instability (with or without long range order), with a magnitude that increases with underdoping, scaling with T^* . The superconducting gap, on the other hand, appears only below T_c on an arc of the Fermi surface around the node that was not removed by the pseudogap, and has a magnitude that decreases with underdoping, scaling with T_c . This can be contrasted with another class of theories that assumes there is a single d -wave pairing gap (not necessarily of the form $\cos k_x a - \cos k_y a$), whose magnitude scales with T^* both in the nodal and antinodal regions. Above T_c , superconducting coherence is destroyed by fluctuations, but gap-like features in the spectral function survive as long as the magnitude of the fermionic damping, $\eta(T)$, is smaller than the angle-dependent pairing self-energy, $\Delta(\phi)$ (specifically, $|\Delta(\phi)| > \sqrt{3}\eta(T)$ ^{2,3}). This gives rise to a T dependent arc around the node, where along the arc, $|\Delta(\phi)|$ is smaller than $\sqrt{3}\eta(T)$, and the spectral function has a peak at the Fermi energy, as in the normal state.

One gap scenarios are consistent with recent photoemission measurements of the temperature dependence of the Fermi arc above T_c ⁴. Measurements by the same group below T_c ⁵ found a simple d-wave gap of the form $\cos 2\phi$ with a magnitude and temperature dependence unrelated to T_c , but consistent with T^* . Similar behavior has been inferred from Fourier transforms of recent scanning tunneling data⁶, except for regions near the node where there is some evidence for a suppressed gap as in earlier photoemission data⁷. A one gap scenario is also consistent with point contact SIS tunneling data⁸.

Recent Raman studies of underdoped Hg -based

cuprates by Le Tacon *et al.*⁹ were interpreted as evidence for the existence of two distinct energy scales in the underdoped cuprates. The Raman spectra in B_{1g} and B_{2g} geometries behave differently with doping: the peak in B_{1g} geometry shifts to a higher energy with underdoping and, to a first approximation, tracks (twice) the antinodal gap, while the peak in B_{2g} geometry shows the same doping dependence as T_c and shifts to a lower energy with underdoping. As B_{1g} and B_{2g} responses predominantly come from the antinodal and nodal regions, respectively¹⁰, this result was interpreted as evidence that the nodal and antinodal gaps have different doping dependences. This does not necessarily imply two distinct gaps (the interpretation of Ref. 9 assumes a d -wave gap with doping dependent anisotropy as in Ref. 7), but still it does imply that the gap function behaves differently in these two momentum regions.

Here, we argue that the Raman data can be explained equally well within a one gap scenario, as a result of final state interactions, which are assumed to increase with underdoping. We find that final state interactions can lead to different doping dependences of the B_{1g} and B_{2g} responses even if the superconducting gap has a simple $\cos 2\phi$ form.

II. FORMALISM

Without final state interactions, the Raman intensity due to electronic excitations is given by the Fermi surface average of the sum of normal (GG) and anomalous (FF) bubbles, weighted with Raman vertices¹¹. In a situation where the self-energy depends only on ω , but not on k normal to the Fermi surface (apart from a trivial velocity renormalization), the Raman intensity at $T = 0$ in the geometry labeled by 'i' is the imaginary part of the Raman bubble: $R_i(\Omega)$, which for $\Omega > 0$ is given by

$$R_i(\Omega) = R_0 \left\langle \gamma_i^2(\phi) \left[2 - \int_{-\infty}^{\infty} d\omega \frac{\sqrt{\tilde{\omega}_+^2 - \Delta^2(\phi)} \sqrt{\tilde{\omega}_-^2 - \Delta^2(\phi)} - \tilde{\omega}_+ \tilde{\omega}_- + \Delta^2(\phi)}{\sqrt{\tilde{\omega}_+^2 - \Delta^2(\phi)} \sqrt{\tilde{\omega}_-^2 - \Delta^2(\phi)} (\sqrt{\tilde{\omega}_+^2 - \Delta^2(\phi)} + \sqrt{\tilde{\omega}_-^2 - \Delta^2(\phi)})} \right] \right\rangle_{FS} \quad (1)$$

where R_0 is a normalization factor, $\tilde{\omega}_{\pm} = \omega_{\pm} - \Sigma(\omega_{\pm})$, $\omega_{\pm} = \omega \pm \Omega/2$, ϕ is the angular variable along the Fermi surface, $\langle \dots \rangle_{FS}$ denotes averaging over the Fermi surface ($\langle \dots \rangle_{FS} = (2/\pi) \int_0^{\pi/2} \dots d\phi$ for a circular Fermi surface), and $\Delta(\phi)$ is the pairing self-energy which for simplicity we assume to be independent of frequency. For a circular Fermi surface, we assume a d -wave gap of the form $\Delta(\phi) = \Delta \cos 2\phi$. The vertices γ_i are different for different scattering geometries and are $\gamma_{B_{1g}}(\phi) = \cos 2\phi$ (i.e., $\cos k_x a - \cos k_y a$), and $\gamma_{B_{2g}}(\phi) = \sin 2\phi$ (i.e., $\sin k_x a \sin k_y a$). Because of the angular dependences of γ_i , B_{1g} Raman scattering predominantly probes the antinodal regions, where $\cos 2\phi$ is the largest, while the B_{2g} Raman intensity comes from the nodal regions, where $\sin 2\phi$ is the largest^{10,11,12}.

In the BCS approximation, $\Sigma = 0$, and the Raman intensity reduces to^{12,13}

$$Im[R_i(\Omega)] = 4\pi R_0 Re \left[\left\langle \frac{\gamma_i^2(\phi) \Delta^2(\phi)}{\Omega \sqrt{\Omega^2 - 4\Delta^2(\phi)}} \right\rangle_{FS} \right] \quad (2)$$

The expressions for $ImR_{B_{1g}}$ and $ImR_{B_{2g}}$ in this approximation can be analytically expressed in terms of complete elliptic integrals¹². At small frequencies, only nodal fermions contribute to the Raman intensity, and

$$ImR_{B_{1g}}(\Omega) = \frac{3\pi}{8} R_0 \left(\frac{\Omega}{v_n} \right)^3, \quad ImR_{B_{2g}}(\Omega) = \frac{\pi}{2} R_0 \frac{\Omega}{v_n} \quad (3)$$

where v_n is the nodal ‘velocity’ ($v_n = 2\Delta$ for a $\cos 2\phi$ gap). The real parts of the $R_{B_{1g}}$ and $R_{B_{2g}}$ bubbles behave as

$$ReR_{B_{1g}}(\Omega) = \frac{1}{3} R_0 \left(\frac{\Omega}{\Delta} \right)^2, \quad ReR_{B_{2g}}(\Omega) = -\frac{1}{3} R_0 \left(\frac{\Omega}{\Delta} \right)^2. \quad (4)$$

At larger frequencies, $ImR_{B_{1g}}(\Omega)$ diverges logarithmically at 2Δ , while $ReR_{B_{1g}}(\Omega)$ jumps from a positive to a negative value:

$$\begin{aligned} ImR_{B_{1g}}(\Omega) &= R_0 \log \frac{2\Delta}{|2\Delta - \Omega|}, \\ ReR_{B_{1g}}(2\Delta + 0) &= -R_0 \left(\pi - \frac{4}{3} \right), \\ ReR_{B_{1g}}(2\Delta - 0) &= \frac{4R_0}{3}. \end{aligned} \quad (5)$$

The B_{2g} intensity ($ImR_{B_{2g}}(\Omega)$) has a broad maximum at around 1.6Δ . The real part of the B_{2g} bubble is negative for all frequencies, and has a weak minimum at 2Δ , where $ReR_{B_{2g}}(\Omega) = -4R_0/3$.

The imaginary and real parts of $R_{B_{1g}}$ and $R_{B_{2g}}$ for general Ω are shown in Figs. 1 and 2.

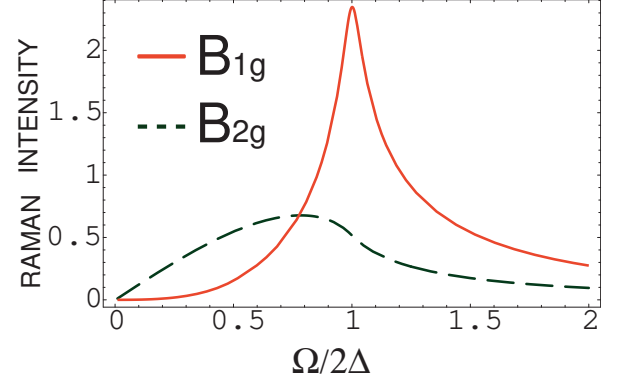


FIG. 1: (Color online) The imaginary part of the Raman bubble, B_{1g} (solid line) and B_{2g} (dashed line), with Ω in units of 2Δ . In the BCS approximation, these are the B_{1g} and B_{2g} Raman intensities. The logarithmic divergence of the B_{1g} intensity at 2Δ is smoothed by the presence of a small damping, $\eta = 0.06\Delta$. Here and in other figures, we plot the Raman intensity in units of $4R_0/\pi$.

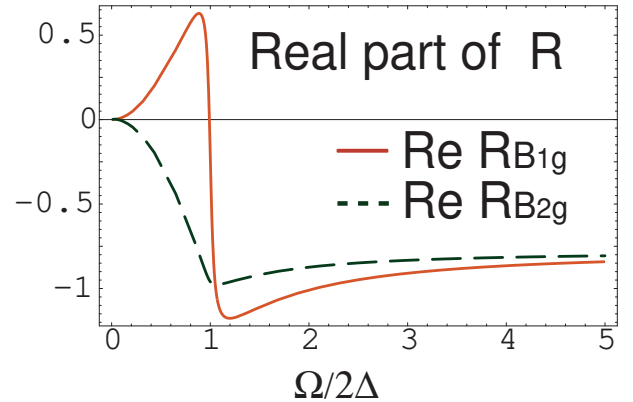


FIG. 2: (Color online) The real part of the Raman bubble, B_{1g} (solid line) and B_{2g} (dashed line). Observe that $ReR_{B_{1g}}$ changes sign, but $ReR_{B_{2g}}$ remains negative for all frequencies.

Final state interactions arise from multiple insertions of the fermion-fermion interaction into the Raman bubble. The fully renormalized four-fermion interaction $\Gamma_{\alpha\beta,\gamma\delta}(q,\Omega)$ generally has components in the spin and charge channels, and depends on the transferred momenta $q = k - k'$ and transferred frequency $\Omega = \omega - \omega'$. Restricting to only B_{1g} and B_{2g} harmonics, we can ap-

proximate Γ as

$$\Gamma_{\alpha\beta,\gamma\delta} = \delta_{\alpha\beta}\delta_{\gamma\delta} \left(\Gamma_{B_{1g}}^c \gamma_{B_{1g}}(k)\gamma_{B_{1g}}(k') + \Gamma_{B_{2g}}^c \gamma_{B_{2g}}(k)\gamma_{B_{2g}}(k') \right) + \sigma_{\alpha\beta}\sigma_{\gamma\delta} \left(\Gamma_{B_{1g}}^s \gamma_{B_{1g}}(k)\gamma_{B_{1g}}(k') + \Gamma_{B_{2g}}^s \gamma_{B_{2g}}(k)\gamma_{B_{2g}}(k') \right) \quad (6)$$

where indices c and s refer to charge and spin, and $\Gamma^{c,s} = \Gamma^{c,s}(\omega - \omega')$.

We make two assumptions in evaluating the effect of final state interactions. First, we assume that the random phase approximation (RPA) is valid, with the full Raman intensity given by

$$\text{Im} \left[\frac{R_i(\Omega)}{1 + \Gamma_i R_i(\Omega)} \right] = \frac{\text{Im} R_i(\Omega)}{(1 + \Gamma_i \text{Re} R_i(\Omega))^2 + (\Gamma_i \text{Im} R_i(\Omega))^2} \quad (7)$$

where $\Gamma_i = \Gamma_i^c + 3\Gamma_i^s$. Second, we assume that the interactions $\Gamma^{c,s}(\Omega)$ depend only weakly on frequency for $\Omega \ll W$, where W is the fermion bandwidth, but are strongly reduced at frequencies comparable to W . This holds if, e.g., the effective interaction is mediated by overdamped spin fluctuations. This is relevant to final state interactions because the constant term in R_i (the ‘2’ in the r.h.s. of Eq. (1)) comes from fermions with energies comparable to W , while the rest comes from fermions with energies of order $\Omega \ll W$. Because the effective interaction is strongly reduced at $\Omega \sim W$, the constant term should be dropped from $\text{Re} R_i$ in the denominator of Eq. (7). At the same time, for the rest of R_i , the interactions Γ^i can be safely approximated by constants¹⁴.

The effect of the final state interactions obviously depends on the sign of Γ_i . The interaction in the B_{1g} channel is the same one as gives rise to d -wave superconductivity. If the spin component of $\Gamma_{B_{1g}}$ dominates over the charge component, $\Gamma_{B_{1g}}$ is negative^{15,16}. $\Gamma_{B_{2g}}$ on the other hand is not related to pairing, and in general can have either sign.

III. RESULTS

A. General d -wave gap

As discussed above, the peak positions in the B_{1g} and B_{2g} Raman intensities as a function of doping do not scale with each other. One way to account for this is to still use the BCS formula, but assume that the gap $\Delta(\phi)$ progressively deviates from the simple $\cos 2\phi$ form with underdoping, such that the gap near the node probed in B_{2g} scattering, and the antinodal gap probed in B_{1g} scattering, have different doping dependences (a ‘two scale’ scenario). A simple way to account for this is to add a $\cos 6\phi$ harmonic to the $d_{x^2-y^2}$ gap function^{7,9}:

$$\Delta(\phi) = \Delta[(1 - a) \cos 2\phi + a \cos 6\phi] \quad (8)$$

Note that the maximum value of the gap is still Δ . In Figs. 3 and 4, we show the B_{1g} and B_{2g} Raman profiles for $a = 0$ and a finite a versus Ω . We see that the peak position in B_{2g} geometry progressively shifts to lower frequencies with increasing a , and flattens. The B_{1g} peak, on the other hand, doesn’t move, but just broadens. Because Δ increases with underdoping, the B_{1g} peak, located at 2Δ , actually shifts to higher frequency with underdoping. The B_{2g} peak, however, shifts to lower frequency with underdoping if the doping dependence of a overshadows the growth of Δ . We also note that the slope of the B_{2g} Raman intensity at $\Omega = 0$ increases with increasing a .

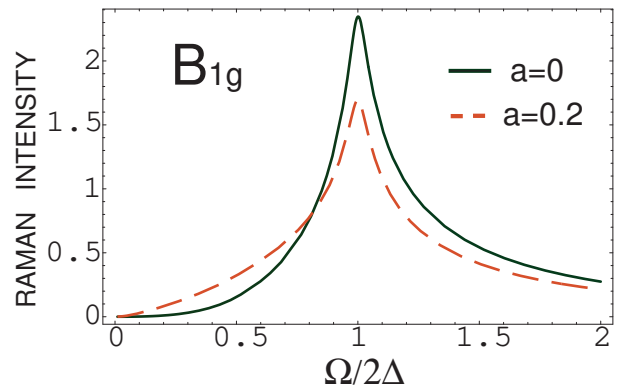


FIG. 3: (Color online) B_{1g} Raman intensity for a gap anisotropy parameter $a = 0$ (solid) and $a = 0.2$ (dashed), with $\eta = 0.06\Delta$. Observe that the peak doesn’t move but just broadens with a .

B. Final state interactions

We now show that final state interactions also lead to distinct behaviors of the B_{1g} and B_{2g} Raman intensities (Figs. 5-8), even for a simple d -wave gap (i.e., $a = 0$). In Fig. 5 we show the B_{1g} Raman intensity for negative $\Gamma_{B_{1g}}$. From here on, we express Γ in units of $\pi/(4R_0)$. As $|\Gamma_{B_{1g}}|$ increases, the B_{1g} peak shifts to a somewhat lower frequency compared to 2Δ , and its intensity decreases. Still, the actual frequency of the B_{1g} peak will increase with underdoping if the increase of Δ overshadows the reduction of the peak frequency relative to 2Δ .

For $\Gamma_{B_{1g}} > 0$, the effect of the final state interaction is opposite – the peak shifts to a higher frequency, and

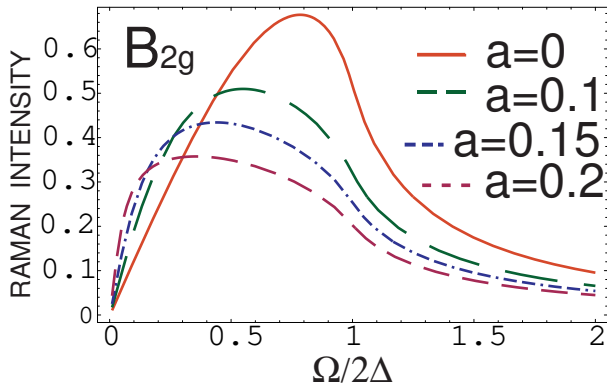


FIG. 4: (Color online) B_{2g} Raman intensity for a gap anisotropy parameter $a = 0, 0.1, 0.15, 0.2$, with $\eta = 0.06\Delta$. The peak moves to lower frequency with increasing a .

its intensity becomes quite large for $\Gamma_{B_{1g}} \sim 1$. For larger $\Gamma_{B_{1g}}$, the intensity drops. We show this behavior in Fig. 6.

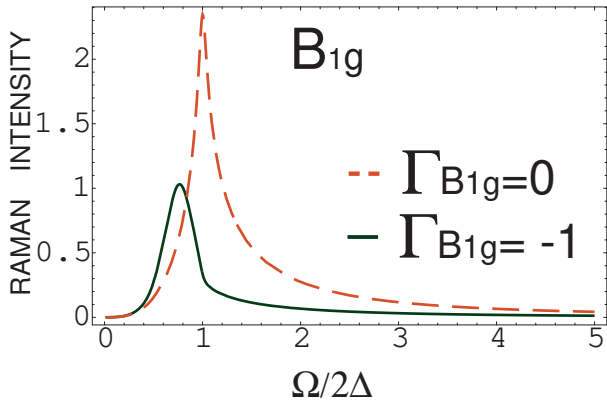


FIG. 5: (Color online) B_{1g} Raman intensity for $\Delta(\phi) = \Delta \cos 2\phi$ with final state interaction $\Gamma_{B_{1g}} = 0$ (dashed) and $\Gamma_{B_{1g}} = -1$ (solid). For finite $\Gamma_{B_{1g}}$, the intensity decreases in magnitude, and the peak shifts to a somewhat lower frequency compared to 2Δ . Here, and in other figures, Γ is expressed in units of $\pi/4R_0$.

We found a stronger effect of the final state interaction in B_{2g} geometry. For negative $\Gamma_{B_{2g}}$, the intensity decreases, and the peak frequency rapidly shifts to a smaller value, demonstrating the same trend as with the gap anisotropy parameter, a . We show this behavior in Fig. 7. The only qualitative difference between this figure and Fig. 4 is that in Fig. 7, the slope of the B_{2g} Raman intensity is unaffected by the final state interaction simply because near $\Omega = 0$, ‘1’ dominates over $R(\Omega)$ in the denominator of Eq. (7).

For positive $\Gamma_{B_{2g}}$ the effect is the opposite – the peak shifts to a larger frequency, and its intensity increases quite dramatically for $\Gamma_{B_{2g}} \sim 1$ (see Fig. 8). For larger $\Gamma_{B_{2g}}$, the intensity drops, and the profile becomes almost flat.

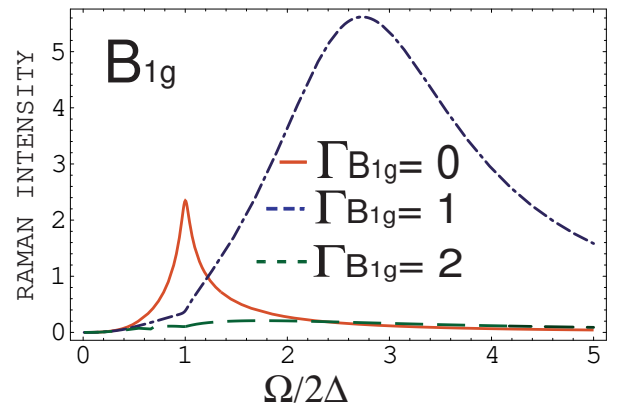


FIG. 6: (Color online) B_{1g} Raman intensity with the final state interaction of opposite sign compared to Fig. 5. The peak shifts to a higher frequency and its intensity increases for $\Gamma_{B_{1g}} \sim 1$. For larger $\Gamma_{B_{1g}}$, the intensity drops.

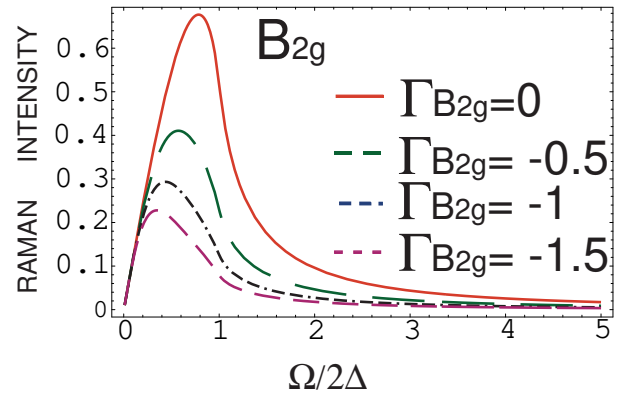


FIG. 7: (Color online) B_{2g} Raman intensity with the final state interaction $\Gamma_{B_{2g}} = 0, -0.5, -1, -1.5$. With increasing $\Gamma_{B_{2g}}$, the peak progressively shifts down in Ω and the intensity decreases. The slope at $\Omega = 0$, however, remains unchanged.

1. Theoretical reasoning

The behavior of the B_{1g} intensity for a d -wave gap in the presence of final state interactions has been studied before^{15,16,17}. The reduction of the peak frequency to below 2Δ for negative $\Gamma_{B_{1g}}$ was understood as an exciton-like effect, similar to the one which gives rise to a peak in the dynamic spin susceptibility in a $d_{x^2-y^2}$ superconductor. $ReR_{B_{1g}}(\Omega)$ is positive below 2Δ and is a monotonic function of Ω in this range (Fig. 2). The denominator of Eq. (7) contains $1 + \Gamma_{B_{1g}} ReR_{B_{1g}}(\Omega)$, and for strong enough, negative $\Gamma_{B_{1g}}$ (from Eq. (5), $|\Gamma_{B_{1g}}| > 3/\pi$), $1 + \Gamma_{B_{1g}} ReR_{B_{1g}}(\Omega)$ equals zero somewhere below 2Δ . In the absence of damping, this would imply a pole, the same as for the spin susceptibility. For the Raman intensity, however, $ImR_{B_{1g}}(\Omega)$ is non-zero for all frequencies. Still, $ImR_{B_{1g}}(\Omega)$ scales as Ω^3 and is generally small below 2Δ . The net result is that the ‘ 2Δ ’ peak shifts to

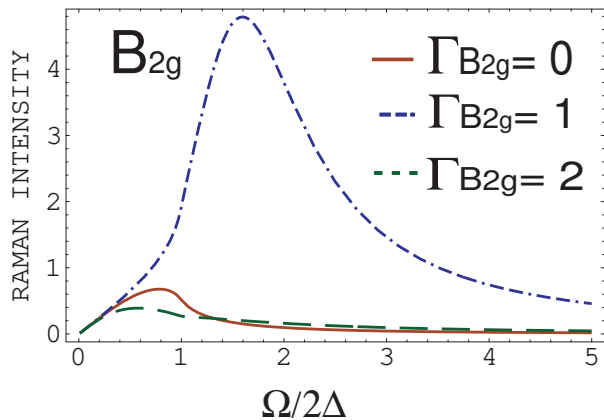


FIG. 8: (Color online) B_{2g} Raman intensity with the final state interaction of opposite sign compared to Fig. 7. The peak shifts to a higher frequency and its intensity increases for $\Gamma_{B_{2g}} \sim 1$ (the same effect as in Fig. 6). For larger $\Gamma_{B_{2g}}$, the intensity drops.

a lower frequency with increasing $|\Gamma_{B_{1g}}|$ ^{15,16}. For large enough $|\Gamma_{B_{1g}}|$, the peak position and the peak intensity scale as $\sqrt{-1/\Gamma}$, as can be easily derived from Eqs. (3), (4), and (7). We note that the intensity of the peak decreases compared to the case with no final state interactions. For $|\Gamma_{B_{1g}}| < 3/\pi$, a pseudo-resonance does not occur. Still, we find the peak position and peak intensity monotonically decrease with increasing $|\Gamma_{B_{1g}}|$.

For the opposite sign of $\Gamma_{B_{1g}}$ ($\Gamma_{B_{1g}} > 0$), there also exists a pseudo-resonance, but this time for $\Omega > 2\Delta$ (Fig. 6). The reason is that $ReR_{B_{1g}}(\Omega)$ changes sign and becomes negative above 2Δ (Fig. 2). For positive $\Gamma_{B_{1g}} \sim 1$, $1 + \Gamma_{B_{1g}} ReR_{B_{1g}}(\Omega)$ crosses zero at some Ω above 2Δ , for which $ImR_{B_{1g}}(\Omega)$ is again small (Fig. 1). For larger positive $\Gamma_{B_{1g}}$, a pseudo-resonance does not develop, and the intensity drops because of the presence of $\Gamma_{B_{1g}}^2$ in the denominator of Eq. (7).

For the B_{2g} case, $ReR_{B_{2g}}(\Omega)$ at small frequencies has the opposite sign (Eq. (4)). Applying the same logic as above, one would then expect a shift of the B_{2g} peak to a lower frequency for $\Gamma_{B_{2g}} > 0$, as in this case $1 + \Gamma_{B_{2g}} ReR_{B_{2g}}(\Omega)$ crosses zero below 2Δ . However, Figs. 7 and 8 show the opposite trend - the peak shifts to a higher frequency for $\Gamma_{B_{2g}} \sim 1$, and to a lower frequency for $\Gamma_{B_{2g}} < 0$. The explanation is that at small frequencies, the imaginary part of $R_{B_{2g}}(\Omega)$ scales linearly with Ω , and is much larger than $ImR_{B_{1g}}(\Omega) \propto \Omega^3$. Because $ImR_{B_{2g}}(\Omega)$ is large, Eq. (7) is not enhanced even when $\Gamma_{B_{2g}} ReR_{B_{2g}}(\Omega) = -1$. In this situation, the trend with positive $\Gamma_{B_{2g}}$ is determined by the fact that $ReR_{B_{2g}}(\Omega)$ doesn't change sign with Ω - it passes through a weak minimum at $\Omega = 2\Delta$ and remains negative at higher frequencies. For $\Gamma_{B_{2g}} \sim 1$, the B_{2g} intensity has a pseudo-resonance at $\Omega > 2\Delta$, just like the B_{1g} intensity does. As the imaginary part of the Raman bubble $ImR_{B_{2g}}(\Omega)$ is small above 2Δ (Fig. 1), the intensity of this pseudo-

resonance is large, and it dominates the profile of the Raman intensity for $\Gamma_{B_{2g}} \sim 1$. For larger $\Gamma_{B_{2g}}$, a pseudo-resonance does not develop ($|\Gamma_{B_{2g}} ReR_{B_{2g}}(\Omega)| > 1$), and the intensity drops, similar to the B_{1g} intensity.

For negative $\Gamma_{B_{2g}}$, a pseudo-resonance does not occur, and the trend with $\Gamma_{B_{2g}} < 0$ is determined by the fact that the final state interaction monotonically decreases the intensity of the B_{2g} Raman response as the frequency increases. At the smallest Ω , this effect is vanishingly small, but for $\Omega \sim 2\Delta$, the intensity is reduced quite substantially. As a result, the B_{2g} Raman intensity develops a maximum at a frequency which becomes smaller as $|\Gamma_{B_{2g}}|$ increases, and the intensity at the maximum progressively decreases, as shown in Fig. 7.

C. Fermionic self-energy

For completeness, we also analyzed the effect of the fermionic self-energy on the Raman profile. As in previous work^{2,3}, we assumed that the self-energy $\Sigma(\omega)$ can be approximated by $\Sigma(\omega) = -i\eta \text{sgn}(\omega)$. In the superconducting state, η is small, but it rapidly increases above T_c and can affect the Raman profile in the pseudogap regime.

The results for the $\cos 2\phi$ gap are shown in Figs. 9 and 10. The peaks in both geometries get broader when damping increases. In addition, the B_{1g} intensity increases at small Ω with increasing η , while the B_{2g} intensity decreases at small Ω . We verified that the same trend persists for a general d-wave gap (i.e., a non-zero), and when final state interactions are included.

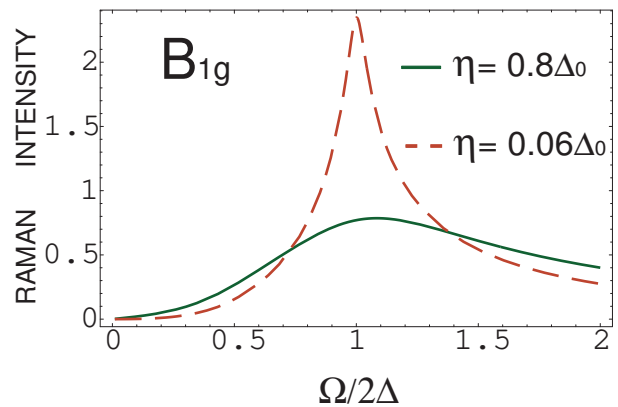


FIG. 9: (Color online) B_{1g} Raman intensity for $\eta = 0.06\Delta$ (dashed) and $\eta = 0.8\Delta$ (solid). With increasing η , the peak broadens, and the intensity at small frequencies increases.

1. Universal slope for B_{2g} intensity

We note in passing that a finite η gives rise to a new universal regime in the B_{2g} response. Namely, for small

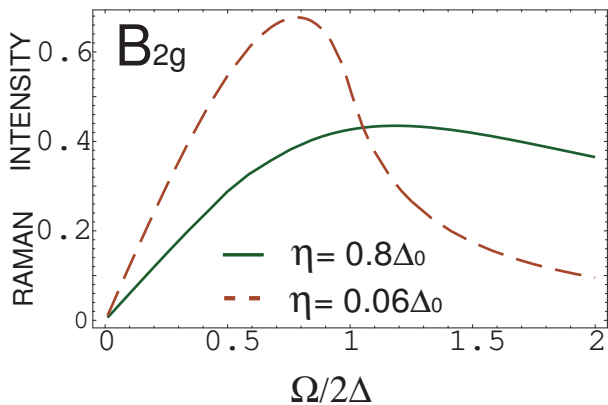


FIG. 10: (Color online) B_{2g} Raman intensity for $\eta = 0.06\Delta$ (dashed) and $\eta = 0.8\Delta$ (solid). The peak broadens and the slope at $\Omega = 0$ decreases.

$\Omega < \eta \ll \Delta$, the B_{2g} Raman intensity is linear in Ω and depends only on the nodal velocity, but is different from that in Eq. (3).

$$ImR_{B_{2g}}(\Omega) = \frac{4}{\pi} R_0 \frac{\Omega}{v_n}, \quad \Omega < \eta \quad (9)$$

This universality of $ImR_{B_{2g}}(\Omega)$ has the same origin as the universal conductivity of a d -wave superconductor¹⁸. We found, however, that this universal behavior sets in only for small $\eta < 0.1\Delta$, while at larger η , the B_{2g} Raman profile at small frequencies is almost independent of the nodal velocity.

IV. COMPARISON WITH EXPERIMENT

We demonstrated that there are two possible ways to explain the Raman data. One explanation assumes that the gap anisotropy changes with underdoping. Another explanation is that the distinct behavior of the B_{1g} and B_{2g} peaks is the effect of final state interactions (Figs. 5 and 7). In both cases, one can reproduce the doping dependences of the B_{1g} and B_{2g} peaks. The second explanation is consistent with recent photoemission data that finds a simple d -wave gap⁵, even in underdoped samples. The qualitative difference between the two scenarios is the behavior of the slope of the B_{2g} Raman response – the slope, measured in units of R_0/Δ , varies with doping via the varying gap anisotropy, but is doping independent if the effect is due to final state interactions.

To extract the doping dependence of the slope from the data, one needs to normalize the theoretical results in the same way as in experiment. Le Tacon *et al.*⁹ normalized the measured Raman response for all dopings by imposing an empirical ‘sum rule’

$$\int d\Omega \Omega ImR_{B_{2g}}(\Omega) = Cp \quad (10)$$

where p is the doping and C is a constant. They argued that this sum rule can be approximately derived for a weakly doped Mott insulator. With this normalization, the slope of $ImR_{B_{2g}}$ is essentially doping independent, although the peak positions in both the B_{1g} and B_{2g} channels vary substantially.

The theoretical Raman intensity contains a prefactor R_0 (see Eq. (1)). It is proportional to the fermionic density of states, N , and the square of the quasiparticle residue, Z . Both N and Z are weakly dependent on doping for overdoped samples, but become doping dependent in the strong coupling regime. The normalization used by Le Tacon *et al.* implies that

$$R_0 \Delta_0^2 \int dz z Im\tilde{R}_{B_{2g}}(z) = Cp \quad (11)$$

where $z = \Omega/\Delta$, and $Im\tilde{R}(z)$ is the function plotted in the figures.

The slope of $ImR_{B_{2g}}(z)$ scales as R_0/Δ if the gap has a simple d -wave form, even if final state interactions are relevant (the final state interaction does not affect the slope). The doping independence of the slope then implies that $R_0 \sim \Delta$. Substituting this into Eq. (11), we find that this is consistent with the data if

$$I(\Gamma_{B_{2g}}) = \int dz z Im\tilde{R}_{B_{2g}}(z) \propto \frac{p}{\Delta^3} \quad (12)$$

At the doping dependence of Δ is known, Eq. (12) is a parameter-free condition that can confirm or disprove our theory. We computed the integral of $Im\tilde{R}_{B_{2g}}$ from Fig. 7 and found $I(0) \approx 0.94$, $I(-1) \approx 0.30$, and $I(-1.5) \approx 0.20$. Extracting the peak position in units of Δ from Fig. 7 and Δ from Fig. 2 of Ref. 9, we find that $\Gamma_{B_{2g}} = 0$ roughly describes the optimal doped $T_c = 95K$ sample ($p = 0.15$), $\Gamma_{B_{2g}} = -1$ the underdoped $T_c = 86K$ sample ($p = 0.12$) for which Δ is about 1.4 times larger than at optimal doping, and $\Gamma_{B_{2g}} = -1.5$ the underdoped $T_c = 63K$ sample ($p = 0.1$) for which Δ is about 1.5 times larger than at optimal doping. Compared to optimal doping, p/Δ^3 in the two underdoped cases is reduced by 0.29 and 0.20, respectively. These numbers are in good agreement with our $I(-1)/I(0) = 0.32$ and $I(-1.5)/I(0) = 0.21$. This good agreement is a strong argument for an explanation based on final state interactions rather than for a strong doping-dependent anisotropy of the gap.

It is instructive to further compare our explanation of the data with the one presented by Le Tacon *et al.*⁹. They included both a $\cos(6\phi)$ contribution to the gap $\Delta(\phi)$ (as in Eq. (8)) and a Fermi liquid renormalization, Λ , of the Raman vertex. They argued that the vertex renormalization factor Λ is angle dependent, $\Lambda = \Lambda_0(1 - C \cos^2 2\phi)$, and that C increases with underdoping. For nodal fermions ($\phi = \pi/4$), the vertex equals Λ_0 and is doping independent, but for antinodal fermions, its values goes down with underdoping. Le Tacon *et al.* argued that they needed the C term to explain the

loss of intensity of the B_{1g} peak, and also to obtain a maximum in the B_{2g} response, which in the absence of the C term is flat.

In our theory, the intensity of the the B_{1g} peak shifts down because of the final state interaction, which is equivalent to the renormalization of the Raman vertex. The suppression in our case is the consequence of the fact that the intensity of the peak scales as $\sqrt{-1/\Gamma}$. In this, we agree with Le Tacon *et al.*. At the same time, the C term in the analysis by Le Tacon *et al.* reduces the B_{1g} vertex for all frequencies, while in our theory, the B_{1g} Raman vertex at the smallest frequencies is enhanced by final state interactions if $\Gamma_{B_{1g}} < 0$ (in Fig. 5, the B_{1g} intensity at small Ω is larger than the one without final state interactions).

In another distinction from Le Tacon *et al.*, the B_{1g} peak in our theory shifts down compared to 2Δ . However, the energy of the peak still increases with underdoping because Δ increases^{10,15,16}.

For B_{2g} scattering, the effect of the C term in their consideration is consistent with our analysis. Namely, their vertex becomes progressively smaller with the deviation of a typical angle ϕ from $\pi/4$. This obviously happens as the frequency increases. In our case, the ratio of the renormalized vertex to the bare one also progressively decreases as the frequency increases, if $\Gamma_{B_{2g}} < 0$. From this perspective, the angular dependence of their C term also mimics the effect of our final state interaction in the B_{2g} channel for a negative sign of $\Gamma_{B_{2g}}$. However, in distinction to Le Tacon *et al.*, we argue that this effect alone explains the data, i.e., there is no need to invoke a doping dependent change of the anisotropy of the d -wave gap.

To be more quantitative, LaTacon *et al.* used the experimental Δ and three other doping dependent parameters: $Z\Lambda_0$, C , and the gap anisotropy parameter, a . Two out of three of these parameters are fixed by (i) the ‘sum rule’ requirement, and (ii) the experimental fact that the slope of the normalized Raman B_{2g} response is doping independent. The one free doping dependent parameter is chosen to fit the position of the B_{2g} peak.

In our theory, we assume a simple d -wave gap and calculated the vertex renormalization based on the RPA¹⁹. We therefore have only two parameters: R_0 , and $\Gamma_{B_{2g}}$ to fit the same three sets of data. As we described above, we found that the agreement with the data is nearly perfect in the sense that once we fix R_0 and $\Gamma_{B_{2g}}$ to match the slope and the peak position in the B_{2g} channel, we find that the experimental normalization condition is satisfied, despite the strong doping variation of Δ .

We also note that the dependence on the fermionic damping in Figs. 9 and 10 is consistent with the data if we assume, like in earlier work^{2,3}, that η increases strongly above T_c . Namely, the maximum in the B_{1g} intensity measured by Le Tacon *et al.* not only shifts, but also broadens with underdoping, and at small Ω the intensity above T_c overshoots the intensity in the superconducting state. For B_{2g} scattering, the intensity in the superconducting state overshoots the intensity in the normal state

in a broad range of frequencies, particularly for the most underdoped $T_c = 63K$ sample (see Fig. 1 of Ref. 9). This behavior is in agreement with Fig. 10.

An issue left in our analysis and in the analysis by LeTacon *et al.* is the justification of the sign of the effective interaction in the B_{2g} channel (this is the sign of $\Gamma_{B_{2g}}$ in our analysis, and the sign of the C term in the analysis of LeTacon *et al.*). To fit the data, we need $\Gamma_{B_{2g}} < 0$. As we said in Sec. II, the full $\Gamma_{B_{2g}}$ has charge and spin components: $\Gamma_{B_{2g}} = \Gamma_{B_{2g}}^c + 3\Gamma_{B_{2g}}^s$. The spin component $\Gamma_{B_{2g}}^s$ has opposite sign compared to $\Gamma_{B_{1g}}^s$ as the interaction is peaked at or near the antiferromagnetic momentum $Q = (\pi, \pi)$. That is, $\Gamma_i^s \propto \gamma_i(k)\gamma_i(p)\chi_s(k-p)$, where k and p are on the Fermi surface, and the sign difference between the B_{2g} and B_{1g} channels is due to the fact that $\gamma_{B_{1g}}(k+Q) = -\gamma_{B_{1g}}(k)$, while $\gamma_{B_{2g}}(k+Q) = \gamma_{B_{2g}}(k)$. If d -wave pairing is magnetically mediated, $\Gamma_{B_{1g}}^s < 0$, hence $\Gamma_{B_{2g}}^s > 0$ (from a pairing perspective, the latter is repulsive). However, the dominant contribution to Γ_s comes from regions near the hot spots, which in the cuprates are rather close to $(\pi, 0)$, for which $\gamma_{B_{2g}} = 0$. As a consequence, the magnitude of $\Gamma_{B_{2g}}^s$ is substantially smaller than that of $|\Gamma_{B_{1g}}^s|$. In this situation, the charge component of the B_{2g} Raman vertex may well exceed the spin component. The charge and spin components of Γ_i contribute with a different sign to the pairing channel (because of the spin factor σ^y in the pairing vertex). Accordingly, the charge-dominated repulsive pairing interaction in the B_{2g} channel corresponds to $\Gamma_{B_{2g}}^c < 0$, and, hence, to a negative $\Gamma_{B_{2g}}$, which we need. In this context, the increase in $|\Gamma_{B_{2g}}|$ with decreasing p well may be a consequence of the reduced screening when approaching the Mott transition.

V. CONCLUSIONS

In summary, we argued in this paper that the data on B_{1g} and B_{2g} Raman scattering by Le Tacon *et al.*⁹ can be explained as an effect of final state interactions, without the need to invoke a doping-dependent change in the anisotropy of the d -wave pairing gap. This work demonstrates that care must be taken when comparing energy gaps derived from two particle spectroscopies like Raman from those obtained directly from ‘single particle’ probes such as photoemission.

Acknowledgments

AVC acknowledges support from nsf-dmr 0604406, from the visitor program of the University of Chicago and Argonne National Laboratory, and is thankful to TU-Braunschweig for their hospitality during the initial stages of this work. MRN was supported by the U. S. Dept. of Energy, Office of Science, under Contract No. DE-AC02-06CH11357. We would like to thank I.

Eremin, M. Randeria, and J.C. Campuzano for useful discussions.

-
- ¹ M. R. Norman, D. Pines and C. Kallin, *Adv. Phys.* **54**, 715 (2005).
- ² M. R. Norman, A. Kanigel, M. Randeria, U. Chatterjee and J. C. Campuzano, *Phys. Rev. B* **76**, 174501 (2007).
- ³ A. V. Chubukov, M. R. Norman, A. J. Millis and E. Abrahams, *Phys. Rev. B* **76**, 180501(R) (2007).
- ⁴ A. Kanigel, M. R. Norman, M. Randeria, U. Chatterjee, S. Souma, A. Kaminski, H. M. Fretwell, S. Rosenkranz, M. Shi, T. Sato, T. Takahashi, Z. Z. Li, H. Raffy, K. Kadowaki, D. Hinks, L. Ozyuzer and J. C. Campuzano, *Nature Phys.* **2**, 447 (2006).
- ⁵ A. Kanigel, U. Chatterjee, M. Randeria, M. R. Norman, S. Souma, M. Shi, Z. Z. Li, H. Raffy and J. C. Campuzano, *Phys. Rev. Lett.* **99**, 157001 (2007).
- ⁶ T. Hanaguri, Y. Kohsaka, J. C. Davis, C. Lupien, I. Yamada, M. Azuma, M. Takano, K. Ohishi, M. Ono and H. Takagi, *Nature Phys.* **3**, 865 (2007); J. C. Davis, private communication.
- ⁷ J. Mesot, M. R. Norman, H. Ding, M. Randeria, J. C. Campuzano, A. Paramekanti, H. M. Fretwell, A. Kaminski, T. Takeuchi, T. Yokoya, T. Sato, T. Takahashi, T. Mochiku and K. Kadowaki, *Phys. Rev. Lett.* **83**, 840 (1999).
- ⁸ J. F. Zasadzinski, L. Ozyuzer, N. Miyakawa, K. E. Gray, D. G. Hinks and C. Kendziora, *Phys. Rev. Lett.* **87**, 067005 (2001).
- ⁹ M. Le Tacon, A. Sacuto, A. Georges, G. Kotliar, Y. Gallais, D. Colson and A. Forget, *Nature Physics* **2**, 537 (2006).
- ¹⁰ G. Blumberg, M. Kang, M. V. Klein, K. Kadowaki and C. Kendziora, *Science* **278**, 1427 (1997).
- ¹¹ T. P. Devereaux and R. Hackl, *Rev. Mod. Phys.* **79**, 175 (2007).
- ¹² T. P. Devereaux and D. Einzel, *Phys. Rev. B* **51**, 16336 (1995).
- ¹³ M. V. Klein and S. B. Dierker, *Phys. Rev. B* **29**, 4976 (1984).
- ¹⁴ The figures are obtained without the constant term. However, we have found that the inclusion of this term does not change the results in any substantial way.
- ¹⁵ A. V. Chubukov, D. K. Morr and G. Blumberg, *Solid State Comm.* **112**, 183 (1999).
- ¹⁶ A. Chubukov, T. P. Devereaux and M. V. Klein, *Phys. Rev. B* **73**, 094512 (2006).
- ¹⁷ T. Dahm, D. Manske, and L. Tewordt, *Phys. Rev. B* **59**, 14740 (1999).
- ¹⁸ P. A. Lee, *Phys. Rev. Lett.* **71**, 1887 (1993).
- ¹⁹ It should be noted that within the RPA, factors such as Z and Λ do not explicitly appear. That is, one uses unrenormalized Greens functions, and the effect of interactions is solely accounted for by Γ .